


# Influence of acceleration on relativistic nonlinear Thomson scattering in tightly focused linearly polarized laser pulses

Yifan Chang(常一凡), Yubo Wang(王禹博), Chang Wang(王畅), Yuting Shen(申雨婷), and Youwei Tian(田友伟)
**Citation:**Chin. Phys. B, 2023, 32 (**6**): 063201. DOI: 10.1088/1674-1056/ac89e6
Journal homepage: http://cpb.iphy.ac.cn; http://iopscience.iop.org/cpb

**What follows is a list of articles you may be interested in**

---

## Asymmetry parameters in single ionization of He, Ne by XUV pulses

Jian-Ting Lei(雷建廷), Xuan Yu(余璇), Guo-Qiang Shi(史国强), Chen-Yu Tao(陶琛玉), Shao-Hua Sun(孙少华), Shun-Cheng Yan(闫顺成), Xin-Wen Ma(马新文), Jing-Jie Ding(丁晶洁), and Shao-Feng Zhang(张少锋)
Chin. Phys. B, 2023, 32 (**5**): 053205. DOI: 10.1088/1674-1056/aca6d9

## umerical studies of isotopic selective photoionization of ytterbium in a three-step ionization scheme

Xiao-Yong Lu(卢肖勇) and Li-De Wang(王立德)
Chin. Phys. B, 2023, 32 (**5**): 053204. DOI: 10.1088/1674-1056/ac9b2f

## Quantum control of ultrafast magnetic field in $H_3^{2+}$ molecules by tricircular polarized laser pulses

Qing-Yun Xu(徐清芸), Yong-Lin He(何永林), Zhi-Jie Yang(杨志杰), Zhi-Xian Lei(雷志仙),Shu-Juan Yan(闫淑娟), Xue-Shen Liu(刘学深), and Jing Guo(郭静)
Chin. Phys. B, 2023, 32 (**3**): 033202. DOI: 10.1088/1674-1056/ac90b6

## Wavelength- and ellipticity-dependent photoelectron spectra from multiphoton ionization of atoms

Keyu Guo(郭珂雨), Min Li(黎敏), Jintai Liang(梁锦台), Chuanpeng Cao(曹传鹏), Yueming Zhou(周月明), and Peixiang Lu((陆培祥)
Chin. Phys. B, 2023, 32 (**2**): 023201. DOI: 10.1088/1674-1056/ac9b36

## Numerical studies of atomic three-step photoionization processes with non-monochromatic laser fields

Xiao-Yong Lu(卢肖勇), Li-De Wang(王立德), and Yun-Fei Li(李云飞)
Chin. Phys. B, 2022, 31 (**6**): 063203. DOI: 10.1088/1674-1056/ac490b

---

# Influence of acceleration on relativistic nonlinear Thomson scattering in tightly focused linearly polarized laser pulses

Yifan Chang(常一凡)[1], Yubo Wang(王禹博)[2], Chang Wang(王畅)[1], Yuting Shen(申雨婷)[1], and Youwei Tian(田友伟)[1,†]

[1] *College of Science, Nanjing University of Posts and Telecommunications, Nanjing* 210023, *China*
[2] *Bell Honors School, Nanjing University of Posts and Telecommunications, Nanjing* 210023, *China*

(Received 26 April 2022; revised manuscript received 1 August 2022; accepted manuscript online 16 August 2022)

The influence of acceleration of electrons on relativistic nonlinear Thomson scattering in tightly focused linearly polarized laser pulses is investigated for the first time. In the framework of classical electrodynamics, it is deduced and found that the more severe the change in the electron transverse acceleration, the stronger the asymmetry of the radiation angle distribution, and the greater the transverse acceleration, the greater the radiation energy. Tightly focused, ultrashort, and high-intensity lasers lead to violent electron acceleration processes, resulting in a bifurcated radiation structure with asymmetry and higher energy. Additionally, a change in the initial phase of the laser brings about periodic change of the acceleration, which in turn makes the radiation change periodically with the initial phase. In other cases, the radiation is in a symmetrical double-peak structure. These phenomena will help us to modulate radiation with more energy collimation.

**Keywords:** transverse acceleration, relativistic nonlinear Thomson scattering, tightly focused, radiation angle distribution

**PACS:** 32.80.–t, 03.50.De, 41.60.Cr, 42.50.Hz **DOI:** 10.1088/1674-1056/ac89e6

## 1. Introduction

The past few years have witnessed the development of research on the interaction of high-power lasers with matter,[1–4] especially ultrafast laser physics.[5–8] As an important source of x-rays[9,10] and $\gamma$-rays,[11–13] relativistic nonlinear Thomson scattering (RNTS) is an important research direction in this field, which has a wide range of applications in the fields of biomedicine,[14,15] ultrafast physics, and atomic physics.[16,17]

Thomson scattering is the scattering of an electromagnetic field and a free charged particle. Due to the existence of Doppler frequency shift, Thomson scattering is often nonlinear. In recent years, the spectrum of nonlinear Thomson scattering in a laser field has been the subject of wide research.[18–25] Lee and Cha combined the electron motion trajectories to study and analyze the temporal and spatial characteristics of RNTS.[26] A stationary electron appears as a result of ionization or injection. Wang *et al.* studied the spatial features of radiation induced by a circularly polarized laser and a stationary electron in different situations from the perspective of electron motion trajectories.[27–29] In fact, relative to electron trajectories, transverse acceleration is a more significant factor affecting RNTS radiation.[30,31] Some previous studies have also investigated the acceleration of electron motion.[18,32,33] However, they tend to focus on longitudinal acceleration and ignore transverse acceleration. At the same time, most of these works do not link acceleration to radiation phenomena. In tightly focused laser pulses, the transverse acceleration has a more obvious variation law, which has a more significant effect on the radiation. Therefore, studying the variation of transverse acceleration is more important for understanding and applying RNTS radiation.

In this paper, we start from the electron transverse acceleration, and systematically and comprehensively study the influence of various parameters on the electron transverse acceleration in linearly polarized Gaussian beams and the RNTS radiation features caused by a change in transverse acceleration. Using numerical simulation, the three-dimensional spatial and temporal spectra of radiation are presented for intuitive comparison. Our investigation shows that our work gives the first three-dimensional spatial spectrum of RNTS radiation. We find that the magnitude of transverse acceleration affects the magnitude of radiated energy, and the changing trend of transverse acceleration affects the distribution of radiation angles. The characteristic curves of the maximum radiation energy and the energy asymmetry coefficient with each parameter are obtained. At the same time, it is found that the RNTS radiation has asymmetry, energy concentration, and periodic variability in tightly focused ultrashort intense linearly polarized laser pulses. For the above phenomenon, we also make an explanation.

The rest of this paper is as follows. In Section 2, we deduce the laser pulse vector potential, the law of electron motion, and the analytical expression of RNTS radiation using classical electrodynamic principles. In Section 3, the effects of the beam waist radius, laser intensity, pulse width, and initial phase on the transverse acceleration of electrons and the spatial and temporal characteristics of radiation are analyzed.

[†]Corresponding author. E-mail: tianyw@njupt.edu.cn

© 2023 Chinese Physical Society and IOP Publishing Ltd 

Section 4 summarizes the magnitude of acceleration on RNTS in tightly focused linearly polarized pulses and puts forward the application prospect of this law.

## 2. Theory and formula

### 2.1. Laser pulses

In tightly focused lasers, the paraxial approximation is no longer valid and higher-order field effects need to be considered. The beam is modeled by a vector potential linearly polarized along $+x$ from which the following electric field components may be derived:[30,31]

$$\begin{aligned} E_x &= E\left\{S_0+\varepsilon^2\left[\zeta^2 S_2-\frac{\rho^4 S_3}{4}\right]\right. \\ &\quad +\varepsilon^4\left[\frac{S_2}{8}-\frac{\rho^2 S_3}{4}-\frac{\rho^2\left(\rho^2-16\zeta^2\right)S_4}{16}\right. \\ &\quad \left.\left.-\frac{\rho^4\left(\rho^2+2\zeta^2\right)S_5}{8}+\frac{\rho^8 S_6}{32}\right]\right\}, \end{aligned} \tag{1}$$

$$E_y = E\zeta v\left\{\varepsilon^2 S_2+\varepsilon^4\left[\rho^2 S_4-\frac{\rho^4 S_5}{4}\right]\right\}, \tag{2}$$

$$\begin{aligned} E_z &= E\zeta\left\{\varepsilon C_1+\varepsilon^3\left[-\frac{C_2}{2}+\rho^2 C_3-\frac{\rho^4 C_4}{4}\right]\right. \\ &\quad +\varepsilon^5\left[-\frac{3C_3}{8}-\frac{3\rho^2 C_4}{8}+\frac{17\rho^4 C_5}{16}\right. \\ &\quad \left.\left.-\frac{3\rho^6 C_5}{16}-\frac{3\rho^6 C_6}{8}+\frac{\rho^8 C_7}{32}\right]\right\}. \end{aligned} \tag{3}$$

Similarly, the magnetic field components are given by

$$B_x = 0, \tag{4}$$

$$\begin{aligned} B_y &= E\left\{S_0+\varepsilon^2\left[\frac{\rho^2 S_2}{2}-\frac{\rho^4 S_3}{4}\right]\right. \\ &\quad \left.+\varepsilon^4\left[-\frac{S_2}{8}+\frac{\rho^2 S_3}{4}+\frac{5\rho^4 S_4}{16}-\frac{\rho^6 S_5}{4}+\frac{\rho^8 S_6}{32}\right]\right\}, \end{aligned} \tag{5}$$

$$\begin{aligned} B_z &= Ev\left\{\varepsilon C_1+\varepsilon^3\left[\frac{C_2}{2}+\frac{\rho^2 C_3}{2}-\frac{\rho^4 C_4}{4}\right]\right. \\ &\quad \left.+\varepsilon^5\left[\frac{3C_3}{8}+\frac{3\rho^2 C_4}{8}+\frac{3\rho^4 C_5}{16}-\frac{\rho^6 C_6}{4}8+\frac{\rho^8 C_7}{32}\right]\right\}. \end{aligned} \tag{6}$$

Note that a cross section through the beam focus is circular and has a radius $b_0$; a cross section through an arbitrary point $z$ on the axis is also circular with a radius given by $b(z)=b_0\sqrt{1+(z/z_{\mathrm{R}})^2}$. With $k=2\pi/\lambda$, the Rayleigh length is $z_{\mathrm{R}}=kb_0^2/2$ and the diffraction angle is $\varepsilon=b_0/z_{\mathrm{R}}$. In Eqs. (1)–(6), $\xi=x/b_0 v=y/b_0$, and

$$E=E_0\frac{b_0}{b}\exp\left[-\frac{\eta^2}{L^2}-\frac{r^2}{b^2}\right],\quad E_0=kA_0, \tag{7}$$

$L$ is the pulse width and is related to the beam duration. $L=\tau c$, where $\tau$ is the laser duration.

$$a_0=eA_0/(mc^2), \tag{8}$$

$$S_n=\left(\frac{b_0}{b}\right)^n\sin\left(\xi+n\xi_{\mathrm{G}}\right),\quad n=0,1,2,\ldots, \tag{9}$$

$$C_n=\left(\frac{b_0}{b}\right)^n\cos\left(\xi+n\xi_{\mathrm{G}}\right), \tag{10}$$

$$\boldsymbol{E}=-\frac{1}{c}\frac{\partial\boldsymbol{A}}{\partial t},\quad \boldsymbol{B}=\nabla\times\boldsymbol{A}. \tag{11}$$

Furthermore, $k=\omega/cr^2=x^2+y^2$, and $\rho=r/b_0$. These equations were derived from a vector potential with an amplitude $A_0$ and a frequency $\omega$. Additionally, $\xi=\xi_0+\xi_{\mathrm{p}}-\xi_R+\xi_{\mathrm{G}}$, where $\xi_0$ is a constant phase, $\xi_{\mathrm{p}}=\eta=\omega t-kz$ is the plane wave phase, $\xi_{\mathrm{G}}=\tan^{-1}(z/z_{\mathrm{R}})$ is the Gouy phase associated with the fact that a Gaussian beam undergoes a total phase change of $\pi$ as $z$ changes from $-\infty$ to $+\infty$, $\xi_R=kr^2/(2R)$ is the phase associated with the curvature of the wave fronts, and $R(z)=z+z_{\mathrm{R}}^2/z$ is the radius of curvature of a wave front intersecting the beam axis at the coordinate $z$. The fields given above satisfy Maxwell's equations $\nabla\cdot\boldsymbol{E}=0=\nabla\cdot\boldsymbol{B}$, plus terms of order $\varepsilon^6$.

Our paper is based on single-electron theory. We discuss the dynamics of the electron, of mass $m$ and charge $-e$, by numerically solving the equations

$$\frac{\mathrm{d}\boldsymbol{p}}{\mathrm{d}t}=-e\left[\boldsymbol{E}+\boldsymbol{u}\times\boldsymbol{B}\right],\quad \frac{\mathrm{d}\kappa}{\mathrm{d}t}=-ec\boldsymbol{u}\cdot\boldsymbol{E}. \tag{12}$$

In Eq. (10) the quantities have their usual definitions: momentum $\boldsymbol{p}=\gamma mc\boldsymbol{u}$, energy $\kappa=\gamma mc^2$, Lorentz factor $\gamma=\left(1-\boldsymbol{u}^2\right)^{-1/2}$, and the velocity, normalized by the speed of light $c$ in a vacuum, is $\boldsymbol{u}$. The peak field intensity $I_0$ is expressed in terms of $q=eE_0/(mc\omega)$, where $I_0\lambda^2\approx 1.375\times 10^{18}q^2\ (\mathrm{W/cm^2})\cdot\mu\mathrm{m}^2$.

In the space coordinate system, the radiation direction vector can be written as $\boldsymbol{n}=(\sin\theta,\cos\phi,\sin\theta\sin\phi,\cos\theta)$, where $\theta$ means the angle to the laser movement direction, and $\phi$ represents the deflection azimuth angle on the plane perpendicular to the origin point shown in Fig. 1.

There are three equations to discuss the radiation spectrum and power of a single electron as follows.[34] At time $t$, the radiated power normalized by $e^2\omega^2/(4\pi c)$ per unit solid angle is

$$\frac{\mathrm{d}P(t)}{\mathrm{d}\Omega}=\left|\frac{|\boldsymbol{n}\times[(\boldsymbol{n}-\boldsymbol{u})\times d_t\boldsymbol{u}]|^2}{(1-\boldsymbol{u}\cdot\boldsymbol{n})^6}\right|_{t'}, \tag{13}$$

with $t=t'+s_0-n\cdot r$. $t'$ is the electron time or retardation time. $s_0$ is the distance from the origin to the observer and $r$ is the position vector of the electron. The radiation energy accumulation over each solid angle is the integral of the radiant power over time, namely,

$$\frac{\mathrm{d}W}{\mathrm{d}\Omega}=\int_{-\infty}^{+\infty}\frac{|\boldsymbol{n}\times[(\boldsymbol{n}-\boldsymbol{u})\times d_t\boldsymbol{u}]|^2}{(1-\boldsymbol{u}\cdot\boldsymbol{n})^6}\mathrm{d}t, \tag{14}$$

$$\frac{\mathrm{d}P(t)}{\mathrm{d}\Omega}\Big|_{\mathrm{peak}}\approx\frac{e^2}{4\pi c}\left\{\frac{|d_t\boldsymbol{u}_{\boldsymbol{x}}|^2}{(1-\boldsymbol{u})^4}\right\}_{t'}\propto\left\{\gamma^8|d_t\boldsymbol{u}_{\boldsymbol{x}}|^2\right\}_{t'}. \tag{15}$$

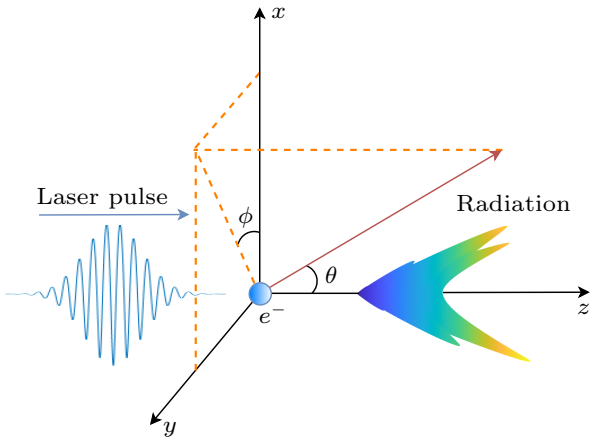



**Fig. 1.** Schematic of relativistic nonlinear Thomson scattering.

## 3. Numerical results

Our laser wavelength $\lambda_0$ is 1 μm, and the radiation is observed on a spherical surface with a radius of 1 m with the origin of the coordinates as the center. When studying the variation of transverse acceleration, the process of electron–laser interaction is normalized by the total interaction time. In order to facilitate the comparison of different situations, the radiation spatial angular distribution of RNTS is normalized and projected onto a plane perpendicular to the laser propagation direction (shown in Fig. 2). In the plot of the radiation space spectrum, the color and height represent the radiation energy. To quantitatively describe the asymmetry of the spatial distribution of radiation, the energy asymmetry coefficient is applied, which means the ratio of the primary peak to the main peak of radiation. The smaller its value, the stronger the radiation asymmetry. The maximum radiation angle refers to the $\theta$ value of the observation point with the largest cumulative radiation energy relative to the origin in the entire RNTS process described in the spherical coordinate system. The ray direction from the origin through this observation point is the direction of maximum radiation. The maximum radiation energy is defined as the radiation energy in the direction of the maximum radiation angle. We characterize the laser intensity by the maximum amplitude $a_0$ of the laser pulsed electromagnetic wave. The relationship between maximum amplitude and intensity $I$ is $a_0 = 0.85 \times 10^{-9}\lambda_0\sqrt{I}$.

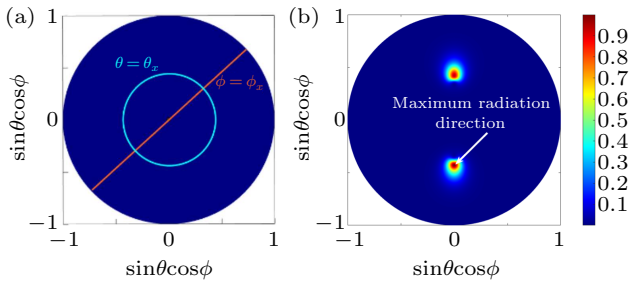



**Fig. 2.** Schematic of angles in the radiation space spectrum.

### 3.1. Beam waist

There are two obvious characteristics of the electron transverse acceleration change process. With an increase in time, the transverse acceleration of electrons fluctuates first and then decreases. There is a certain interval between two adjacent acceleration peaks in opposite directions of electron motion. It can be seen from Fig. 3 that when the beam waist radius is slightly larger (that is, $b_0 \geq \lambda_0$), the acceleration curve of the electron motion almost coincides. This is consistent with what was previously found in RNTS of circularly polarized lasers.[25] The motion state of the electron is very similar to that in a plane wave (with an infinite beam waist radius). Similar acceleration processes imply similar spatial distribution of radiation. Figure 4 shows the radiation space distribution of $b_0 = 6\lambda_0$ and RNTS in plane waves. Apparently, they are very similar in spatial structure, which is an asymmetric double-peak structure.

As the beam waist radius decreases, the acceleration process of electrons begins to change significantly. Nonlinear characteristics begin to manifest in the spatial distribution of radiation. The characteristic of tightly focused laser pulses is that the effects of longitudinal fields become very pronounced compared to plane waves. At the same time, the influence of some higher-order terms of the laser on electron motion and radiation cannot be ignored. In Fig. 3, it can be clearly seen that when $b_0 = 2\lambda_0$, the acceleration decays very quickly in the later stage of the relativistic drift motion of the electron. The acceleration decay rate of electron motion in a tightly focused laser is greater than that in a non-tightly focused laser. The spatial distribution of radiation also begins to bifurcate.

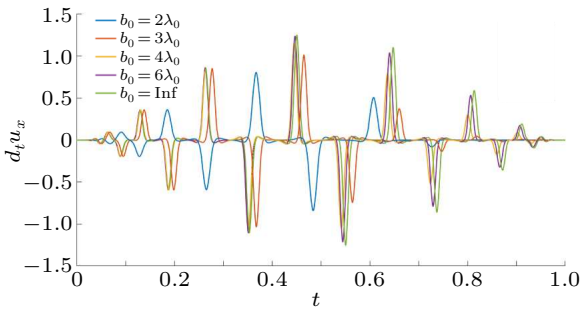



**Fig. 3.** Transverse acceleration of electron motion in lasers with different beam waists. Here, the maximum laser pulse amplitude $a_0 = 8$, the pulse width $L = 3\lambda_0$, and the initial phase $\xi_0 = 0$.

It can be seen from the formula of the laser pulse vector field in Eqs. (3) and (4) that the smaller the value of the beam waist radius, the more severe the change in the vector potential with the position. Simplifying the vector field formulation shows that $b_0$ is in the denominator. This means that the smaller $b_0$ is, the greater the impact of its changes. This property is also reflected in the quantitative analysis of the radiation asymmetry coefficient and maximum energy. It can be seen from Fig. 5 that the radiation asymmetry coefficient increases

sharply with an increase in the beam waist radius, and then decreases slowly after reaching the peak at $b_0 = 4\lambda_0$. The maximum radiation energy increases monotonically, which is consistent with the increase in the maximum acceleration value of electron motion with increasing beam waist radius. It is worth noting that the radiation energy first increases and then decreases with increasing beam waist radius. This is consistent with the change in electron transverse acceleration. It can be seen from Fig. 5 that the maximum transverse acceleration of electron motion increases with an increase in the beam waist radius, and the increase is smaller and smaller. When $b_0 < 4\lambda_0$, $\mathrm{d}W/\mathrm{d}\Omega \propto b_0^2$, and when $b_0 \geq 4\lambda_0$, $\mathrm{d}W/\mathrm{d}\Omega \propto \ln b_0$.

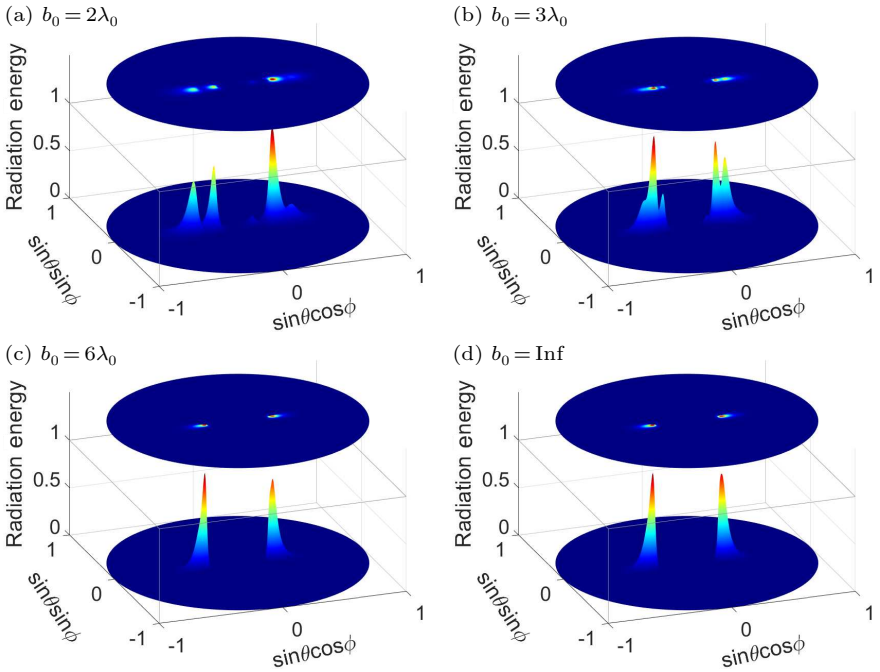



**Fig. 4.** Radiated energy angular distribution in lasers with different beam waists. Here, the maximum laser pulse amplitude $a_0 = 8$, the pulse width $L = 3\lambda_0$, and the initial phase $\xi_0 = 0$.

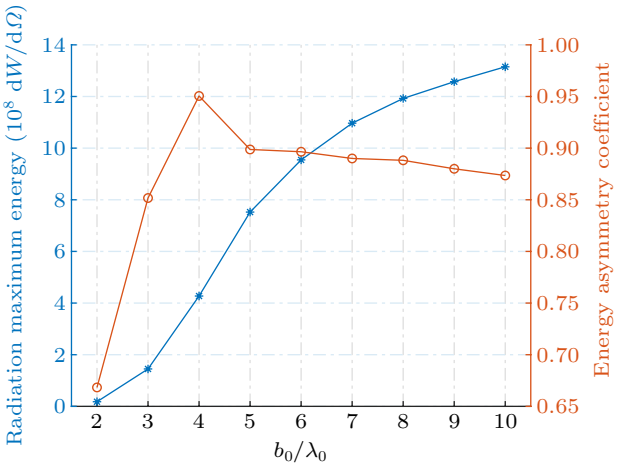



**Fig. 5.** Variation of maximum radiation energy and energy asymmetry coefficient with beam waist radius.

In conclusion, the RNTS radiation in linearly polarized light is convergent as the beam waist radius increases. Radiation spatial distribution characteristics and energy values converge to the case of plane waves. The radiation in the tightly focused laser has obvious nonlinear characteristics and rich properties, which we will study and analyze in detail in the following.

Existing ultrashort ultra-intense laser pulses are mostly tightly focused laser pulses[25,28] because, in the laboratory, the generation of non-tightly focused lasers (plane waves) consumes huge amounts of energy, while tightly focused lasers consume relatively little energy. At the same time, in our study, it can also be found that when the beam waist radius increases to a certain extent, the radiation properties of RNTS hardly change with the beam waist radius. Therefore, exploring RNTS in tightly focused laser pulses has important guiding significance for both theoretical research and experiments.

### 3.2. Laser intensity

The effect of increasing the laser intensity on the laser pulse is that the value of the vector potential becomes larger. Since $a_0$ is on the exponential term coefficient of the vector potential, an increase in $a_0$ will cause the vector potential to change more violently with the position; that is, the gradient will become larger. For electrons, the drift motion along the laser propagation direction will become significant under the action of strong laser light, even comparable to the speed of light.

It is evident from Fig. 6 that, as the laser intensity increases, the electron motion driven by the stronger laser pulse has a higher local maximum value of transverse acceleration in the oscillation increasing stage. After reaching the maxi-

mum value of the whole process, the acceleration of electron motion in the stronger laser will decrease sharply by a larger magnitude. The process of electron movement in a laser pulse consists of two stages. In the first stage, the transverse acceleration of the electron fluctuates upwards and eventually reaches its maximum. In the second stage, the transverse acceleration value fluctuations of the electrons decrease. When the laser intensity is large ($a > 5$), in the first stage, the transverse acceleration of the electron motion has a greater transverse acceleration value and increased amplitude. However, in the second stage, when $a > 5$, the transverse acceleration decreases greatly, and the value of the transverse acceleration becomes very small. When $a_0 > 5$, the greater the laser intensity, the smaller the local maximum transverse acceleration, even smaller than the case of $a_0 < 5$. This means that greater laser intensities cause more drastic changes in electron acceleration. This is self-consistent with our deduction from the point of view of the laser pulse vector potential (i.e., stronger laser means larger gradient).

The drastic change in transverse acceleration leads to the nonlinear nature of the radiation, mainly manifested as energy collimation and asymmetry. As can be seen from Fig. 7, an increase in the laser intensity leads to a smaller radiation angle range. After $a_0$ is greater than 6, the spatial distribution of radiation appears bifurcated. Since the relationship between transverse acceleration and radiated power and energy has been derived, it can be seen that larger transverse acceleration peaks mean stronger attosecond pulses (from the previous work, it is clear that the radiation emits an attosecond pulse).[35] Due to the extremely high relativistic drift velocity of electrons, it can be seen from the time spectrum of the radiation in Fig. 8 that the time distribution of the radiation becomes more distorted. The drastic changes in transverse acceleration result in huge energy differences in radiation from different angles. The radiation energy is decoupled. The asymmetry is mainly because the increase in the strength causes the vector potential gradient to become larger, and the acceleration difference at different positions is huge, so the asymmetry appears. It can also be observed from Fig. 8 that the radiation power increases with the laser intensity. This is compounded with the previous formula ($P \propto \gamma^2 F_\perp^2$).[34]

As the laser intensity increases, the relativistic drift motion of electrons along the direction of laser propagation (positive $z$-axis) becomes increasingly pronounced. This not only results in an increase in radiation power and energy, but also makes the full spatial distribution of radiation more inclined to the $z$-axis. The elevation angle $\theta$ of the maximum radiation direction also decreases with an increase in $a_0$. Through the formula $\arctan\theta = u_\perp/u_z$, we can foresee the existence of this phenomenon.

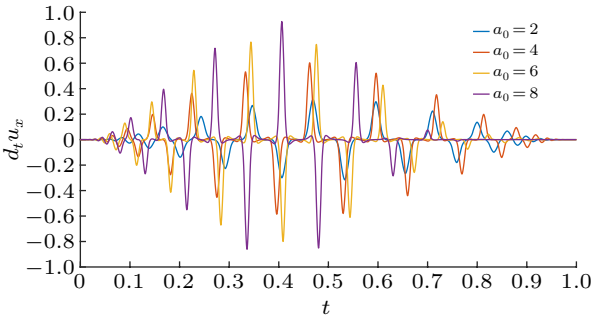



**Fig. 6.** Transverse acceleration of electron motion in lasers with different laser intensities. Here, the beam waist $b_0 = 3\lambda_0$, the pulse width $L = 3\lambda_0$, and the initial phase $\xi_0 = 0$.

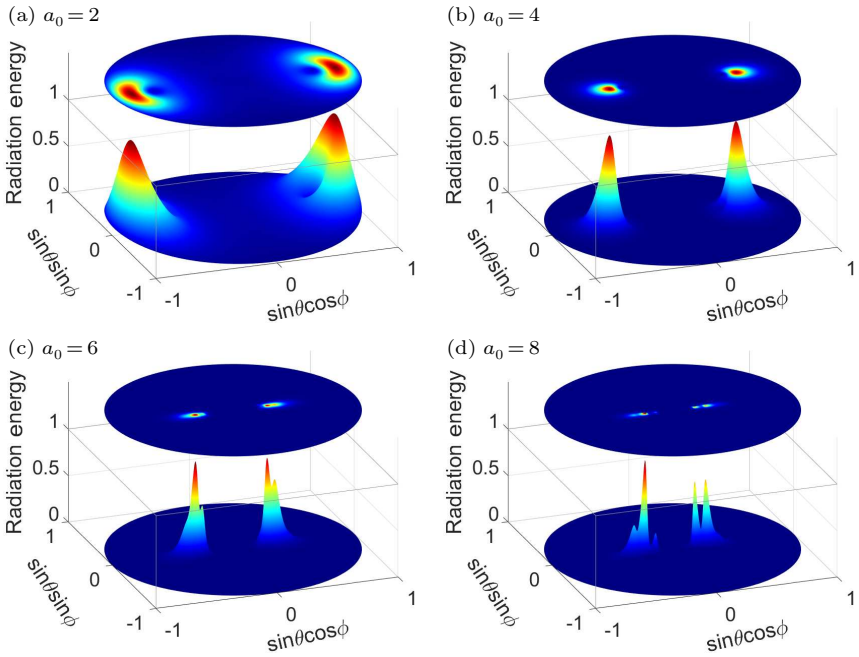



**Fig. 7.** Radiated energy angular distribution in lasers with different laser intensities. Here, the beam waist $b_0 = 3\lambda_0$, the pulse width $L = 3\lambda_0$, and the initial phase $\xi_0 = 0$.

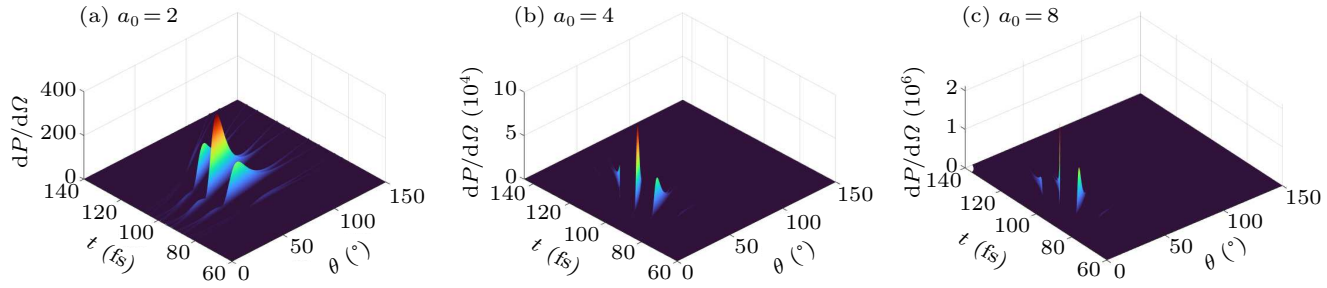



**Fig. 8.** Time distribution in lasers with different laser intensities. Here, the beam waist $b_0 = 3\lambda_0$, the pulse width $L = 3\lambda_0$, and the initial phase $\xi_0 = 0$.

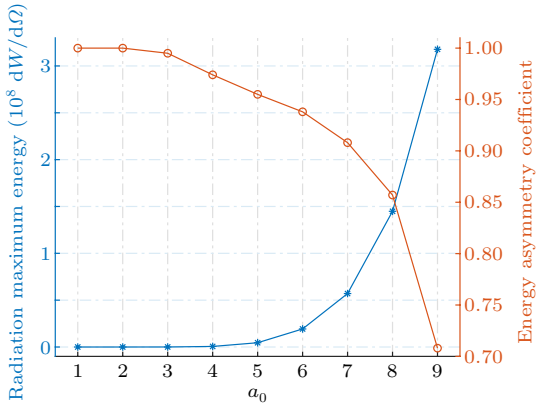



**Fig. 9.** Variation of maximum radiation energy and energy asymmetry coefficient with laser intensity.

Figure 9 shows the variation law of the energy asymmetry coefficient and the maximum radiation energy with $a_0$. Interestingly, the energy asymmetry coefficient and the radiated energy change in almost the same range, but the change trend is opposite. Specifically, the radiation maximum energy increases with an increase in $a_0$, namely, $dW/d\Omega \propto a_0^5$. The energy asymmetry coefficient decreases faster and faster.

### 3.3. Pulse width

In Fig. 10, it can be seen that the increase in pulse width has two effects on the transverse acceleration of electrons. On the one hand, the transverse acceleration has a more intensive number of changes. On the other hand, the maximum transverse acceleration (that is, the amplitude of the transverse acceleration variation) decreases with increasing pulse width. Dense acceleration peaks imply a coupling phenomenon of

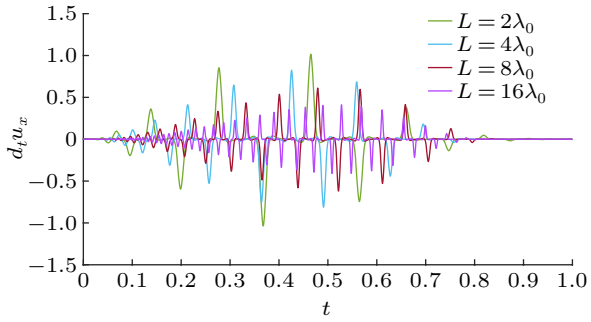



**Fig. 10.** Transverse acceleration of electron motion in lasers with different pulse widths. Here, the beam waist $b_0 = 3\lambda_0$, the maximum laser pulse amplitude $a_0 = 8$, and the initial phase $\xi_0 = 0$.

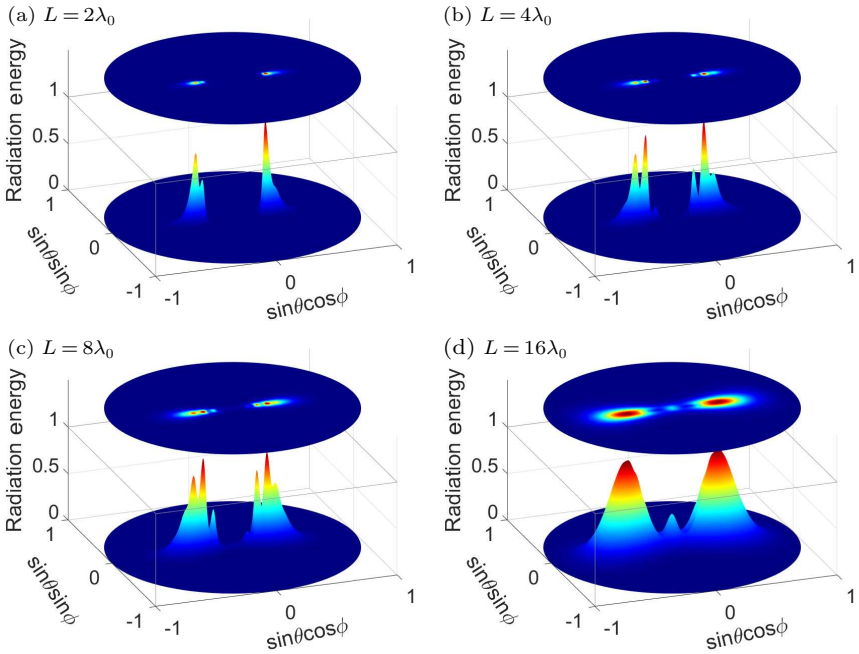



**Fig. 11.** Radiated energy angular distribution in lasers with different pulse widths. Here, the beam waist $b_0 = 3\lambda_0$, the maximum laser pulse amplitude $a_0 = 8$, and the initial phase $\xi_0 = 0$.

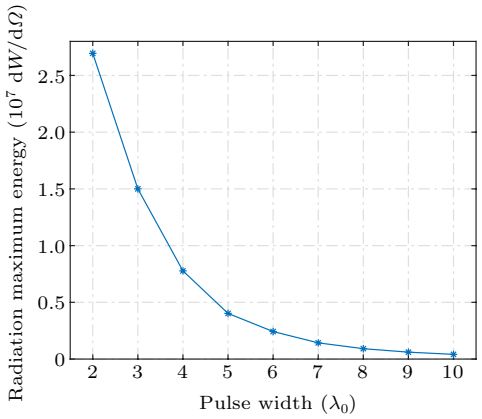



**Fig. 12.** Variation of maximum radiation energy with pulse width.

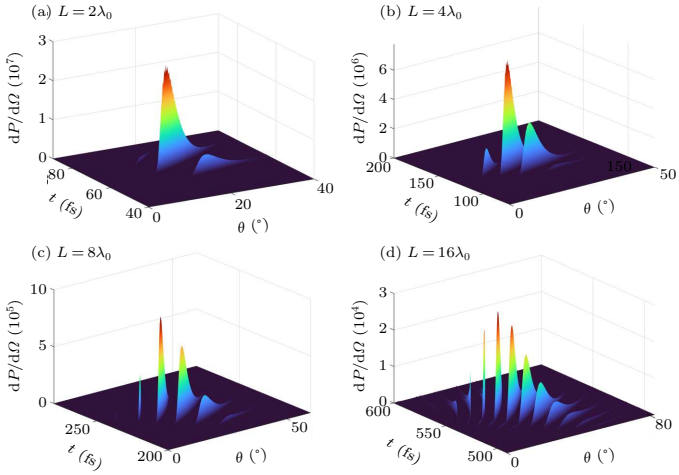



**Fig. 13.** Time distribution in lasers with different laser intensities. Here, the beam waist $b_0 = 3\lambda_0$, the maximum laser pulse amplitude $a_0 = 8$, and the initial phase $\xi_0 = 0$.

radiation, which increases the angular range. The decrease in the transverse acceleration value results in a decrease in the radiated energy.

Obviously, the spatial distribution of the radiated energy in Fig. 11 confirms our inference. The RNTS in the short-pulse laser shows a narrow peak structure. As the pulse width increases, the peaks of the radiation start to couple. Both the angular range of the $\theta$ angle and the angular range of the $\phi$ angle gradually increase. Forks are gradually reduced. Figure 12 shows the radiated maximum power as a function of pulse width. Obviously, the larger the pulse width, the smaller the maximum radiation energy. Mainly, $\mathrm{d}W/\mathrm{d}\Omega \propto \exp\left(-1/L^2\right)$. It is worth noting that the downward trend of the radiated maximum energy is consistent with the position of $L$ in the expression of the laser pulse vector potential, which is the denominator of the negative exponential term $\exp\left(-\eta^2/L^2\right)$ ($\boldsymbol{E} \propto \exp\left(-1/L^2\right)$). The larger $L$ is, the smaller the value of the negative exponential term of $e$ is, and the electromagnetic field of the laser pulse decreases accordingly. The reduction in the laser driving force reduces the transverse acceleration.

The radiated energy of the RNTS unfolded in terms of time, i.e. the power time spectrum, is shown in Fig. 13. It can be seen that the larger the pulse width, the greater the number of radiated attosecond pulses. The radiation also lasts longer. The attosecond pulse radiation power variation in long pulses is gentle, while that in short pulses is drastic. This is the same characteristic as transverse acceleration.

### 3.4. Initial phases

When the pulse width of the laser is greater than $2\lambda_0$, the change in the spatial distribution of radiation with the initial phase of the laser pulse is difficult to detect. In the ultrashort pulse of $L = \lambda_0$, the radiation properties of RNTS have an extremely interesting periodic variation with the initial phase.

From the analysis of the pulse width above, it can be seen that the electrons in the long-pulse laser have more oscillation time. The radiation energy distribution can be viewed as the superposition of multiple attosecond pulses. Therefore, the effect of the initial phase is masked in the constant periodic oscillation. However, the electrons in the ultrashort pulse ($L = \lambda_0$) have very little oscillation time, and the difference between the attosecond pulses is large. Therefore, the effect of the initial phase is well represented.

The $2\pi$ is equally divided into nine different initial phases with $\pi/4$ as the interval in Fig. 14. As can be seen from Fig. 14, the change in the transverse acceleration of the electron motion takes $2\pi$ as a period. That is to say, when the initial phase increases or decreases by an integer multiple of $2\pi$, the variation law of the electron transverse acceleration is exactly the same. When the maxima of the transverse acceleration induced by the laser with different initial phases are connected, a symmetrical Gaussian envelope shape can be seen. Transverse acceleration at intervals of $\pi$ has the exact opposite course of change. Specifically, at the same moment, the transverse acceleration is the same in magnitude and opposite in direction. Electron motion in lasers with initial phases $\pi/2$ and $3\pi/2$ has the highest transverse acceleration maxima.

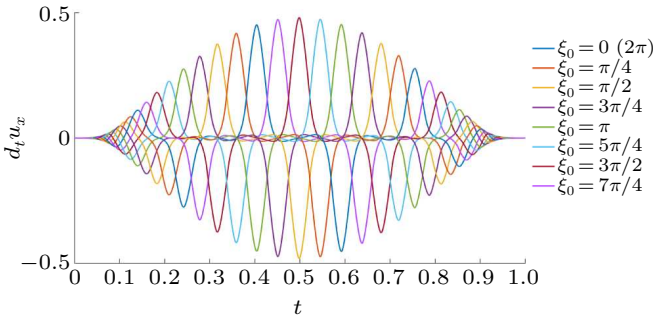



**Fig. 14.** Transverse acceleration of electron motion in lasers with different initial phases. Here, the beam waist $b_0 = 3\lambda_0$, the maximum laser pulse amplitude $a_0 = 8$, and the pulse width $L = \lambda_0$.

Periodic changes in transverse acceleration result in periodic changes in the spatial distribution of radiation. As can be seen from Fig. 16, when the initial phase is between 0 and $\pi$, the radiant energy at $\phi = 0$ keeps decreasing, while the radiant

energy at $\phi = 180^\circ$ keeps increasing. This can be seen as an energy redistribution process. When $\xi_0 = \pi/2$, the radiation has a symmetrical double-peak structure, which means that the two peaks have the same energy. When $\xi_0 > \pi$, the two radiation peaks show opposite trends; that is, the radiation energy at $\phi = 180^\circ$ keeps decreasing, while the radiation energy at $\phi = 0$ keeps increasing. When $\xi_0 = 3\pi/2$, the two peaks show symmetry again.

The change process of the two radiation peaks can be characterized by the change in the energy asymmetry coefficient. The symmetrical periodic variation of the energy asymmetry coefficient can be seen from Fig. 15. Interestingly, the change in the radiated maximum energy and the change in the asymmetry coefficient show an opposite trend, which is $\mathrm{d}W/\mathrm{d}\Omega \propto |\cos\xi_0|$. This process can be understood as the total energy of the two radiation peaks being a constant value, and the asymmetry coefficient reflects the difference in the energy distribution of the two peaks. The stronger the asymmetry, the greater the energy allocated to the larger peak and the greater the maximum radiated energy.

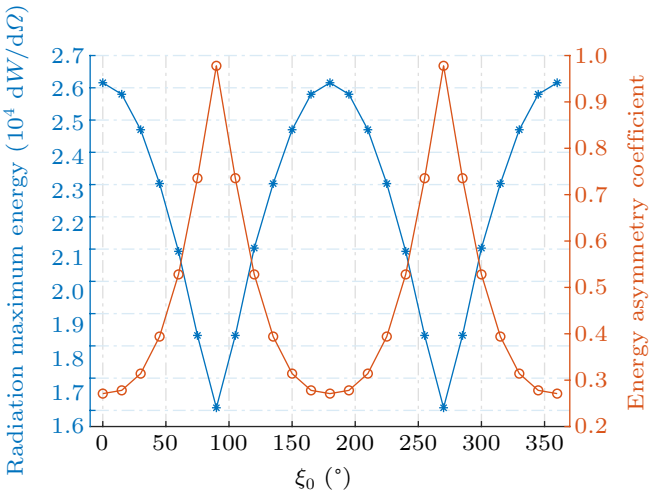



**Fig. 15.** Variation of maximum radiation energy and energy asymmetry coefficient with initial phases.

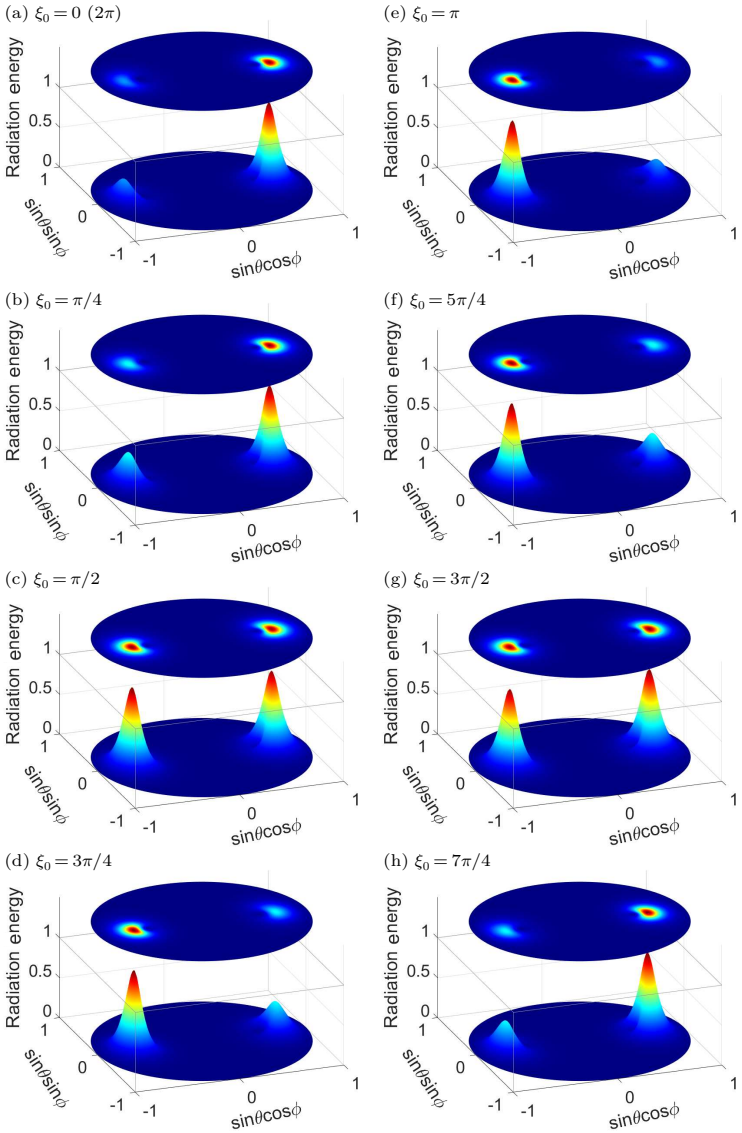



**Fig. 16.** Radiated energy angular distribution in lasers with different initial phases. Here, the beam waist $b_0 = 3\lambda_0$, the maximum laser pulse amplitude $a_0 = 8$, and the pulse width $L = \lambda_0$.

### 3.5. Spectrum

We also study the effects of various parameters on the RNTS spectrum. In Figs. 17–19, we compare the spectrum in the direction of maximum radiation of laser-induced RNTS radiation for different intensities, pulse widths, and beam waist radii. It can be seen that in tightly focused linearly polarized light, the radiation spectrum shows significant nonlinearity. The greater the laser intensity, the shorter the pulse width, the greater the spectral width, and the more obvious the nonlinearity.

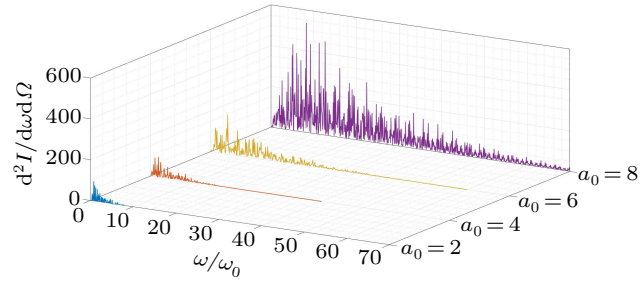



**Fig. 17.** Spectrum in the maximum radiation direction of RNTS in lasers of different intensities, $L=3\lambda_0$, $b=3\lambda_0$.

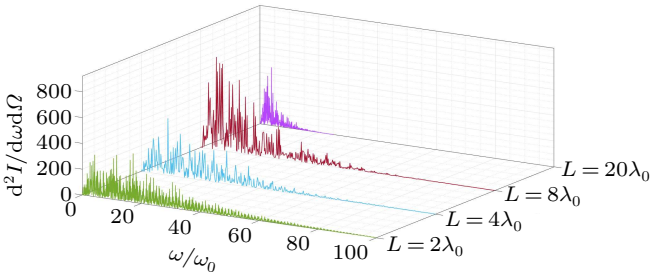



**Fig. 18.** Spectrum in the maximum radiation direction of RNTS in lasers with different pulse widths, $a_0=8$, $b=3\lambda_0$.

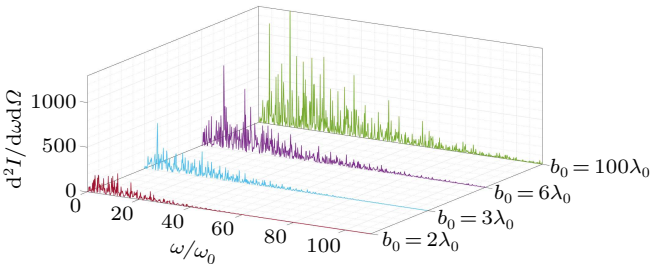



**Fig. 19.** Spectrum in the maximum radiation direction of RNTS in lasers with different beam waist radii, $a_0=8$, $L=3\lambda_0$.

### 3.6. Relationship between maximum transverse acceleration and radiation energy

In addition to the effect of acceleration on the radiation spatial spectrum pattern mentioned above, there is also a quantitative relationship between transverse acceleration and radiation energy. Figure 20 shows the relationship between the maximum radiation energy and the maximum transverse acceleration. It can be clearly seen that the maximum radiation energy of the RNTS increases with an increase in the maximum transverse acceleration. Through data analysis, we find that when the normalized maximum transverse acceleration is less than 0.5, the radiation maximum energy increases linearly with an increase in transverse acceleration ($\mathrm{d}W/\mathrm{d}\Omega \propto |d_t \boldsymbol{u}_x|$). However, when it is greater than 0.5, the maximum radiation energy increases nonlinearly. Namely, $\mathrm{d}W/\mathrm{d}\Omega \propto |d_t \boldsymbol{u}_x|^4$. It can be seen that the case of large acceleration corresponds to nonlinear Thomson scattering, and the nonlinearity of the radiation becomes very obvious.

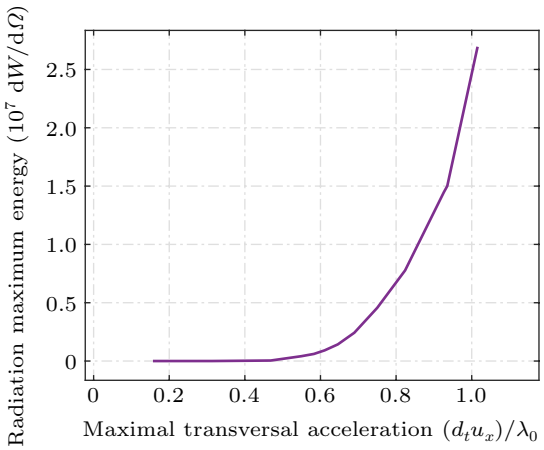



**Fig. 20.** Variation of maximum radiation energy with maximum transverse acceleration.

## 4. Conclusion and perspectives

In this paper, we study the RNTS radiation properties in tightly focused linearly polarized Gaussian laser pulses with different parameters from the perspective of transverse acceleration. The magnitude, direction, and changing frequency of transverse acceleration play a decisive role in the spatial and temporal properties of radiation. Using numerical simulations, we find that the RNTS radiation in tightly focused laser pulses has a more pronounced nonlinearity. Specifically, under strong laser, the radiation has asymmetry and energy collimation. The radiation in ultrashort pulses has obvious asymmetry. Longer pulses lead to more radiation attosecond pulses coupled with radiation. When the pulse width $L=\lambda_0$, the initial phase has an obvious periodic effect on the radiation. Radiation in linearly polarized pulses has the advantage of good energy concentration. Using the laws we discovered, higher-energy, better-collimated radiation can be obtained by adjusting the laser intensity, pulse width, and initial phase. Our work is of great significance for further understanding the mechanism of RNTS and better utilization of RNTS (such as ray sources).

## Acknowledgments

Project supported by the National Natural Science Foundation of China (Grant Nos. 10947170/A05 and 11104291), Natural Science Fund for Colleges and Universities in Jiangsu Province (Grant No. 10KJB140006), Natural Sciences Foundation of Shanghai (Grant No. 11ZR1441300), and Natu-

ral Science Foundation of Nanjing University of Posts and Telecommunications (Grant No. NY221098), and sponsored by the Jiangsu Qing Lan Project and STITP Project (Grant No. XYB2013012).

## References


[1] Maine P, Strickland D, Bado P, Pessot M and Mourou G 1988 *IEEE J. Quant. Electron.* **24** 398

[2] Perry M D and Mourou G 1994 *Science* **264** 917

[3] Eidam T, Hanf S, Seise E, Andersen T V, Gabler T, Wirth C, Schreiber T, Limpert J and Tünnermann A 2010 *Opt. Lett.* **35** 94

[4] Jiang W C and Tian X Q 2017 *Opt. Express* **25** 26832

[5] Mourou G A 1998 *Phys. Today* **51** 22

[6] Corkum P B and Krausz F 2007 *Nat. Phys.* **3** 381

[7] Krausz F and Ivanov M 2009 *Rev. Mod. Phys.* **81** 163

[8] Liang J, Jiang W, Liao Y, Ke Q, Yu M, Li M, Zhou Y and Lu P 2021 *Opt. Express* **29** 16639

[9] Pogorelsky I V, Ben-Zvi I, Hirose T, Kashiwagi S, Yakimenko V, Kusche K, Siddons P, Skaritka J, Kumita T, Tsunemi A, Omori T, Urakawa J, Washio M, Yokoya K, Okugi T, Liu Y, He P and Cline D 2000 *Phys. Rev. Spec. Top. - Accel. Beams* **3** 090702

[10] W L, Tp Y, M C, Ym S, Zc Z, Yy M and Hb Z 2014 *Opt. Express* **22**

[11] Sakai I, Aoki T, Dobashi K, Fukuda M, Higurashi A, Hirose T, Iimura T, Kurihara Y, Okugi T, Omori T, Urakawa J, Washio M and Yokoya K 2003 *Phys. Rev. Spec. Top. - Accel. Beams* **6** 091001

[12] Yan W, Fruhling C, Golovin G, Haden D, Luo J, Zhang P, Zhao B, Zhang J, Liu C, Chen M, Chen S, Banerjee S and Umstadter D 2017 *Nat. Photonics* **11** 514

[13] Liu Y Y, Salamin Y I, Dou Z K, Xu Z F and Li J X 2020 *Opt. Lett.* **45** 395

[14] Suortti P and Thomlinson W 2003 *Phys. Med. Biol.* **48** R1

[15] Chi Z, Du Y, Huang W and Tang C 2020 *J. Synchrotron Radiat.* **27** 737

[16] Lee K, Chung S Y, Park S H, Jeong Y U and Kim D 2010 *Europhys. Lett.* **89** 64006

[17] Baltuska A, Udem T, Uiberacker M, Hentschel M, Goulielmakis E, Gohle C, Holzwarth R, Yakovlev V S, Scrinzi A, Hänsch T W and Krausz F 2003 *Nature* **421** 611

[18] Galkin A, Korobkin V, Romanovsky M and Shiryaev O 2007 *Quant. Electron.* **37** 903

[19] Gao J 2005 *Phys. Rev. Lett.* **93** 243001

[20] Zheng J, Sheng Z M, Zhang J, Wei Z and Yu W 2005 *Acta Phys. Sin.* **54** 1018 (in Chinese)

[21] Vais O, Bochkarev S G and Bychenkov V 2016 *Nonlinear Thomson scattering of a relativistically strong tightly focused ultrashort laser pulse*

[22] Zhu J and Xie B 2019 *J. Opt. Soc. Am. B*

[23] Zhu J and Xie B S 2019 *Europhys. Lett.* **126** 34001

[24] Borovskiy A V and Galkin A L 2021 *Laser Phys. Lett.* **18** 066002

[25] Wang Y, Zhou Q, Zhuang J, Yu P and Tian Y 2021 *Opt. Express* **29** 22636

[26] Lee K, Cha Y, Shin M, Kim B and Kim D 2003 *Opt. Express* **11** 309

[27] Wang Y, Wang C, Zhou Q, Li L and Tian Y 2020 *Laser Phys.* **31** 015301

[28] Wang Y, Wang C, Li K, Li L and Tian Y 2020 *Laser Phys. Lett.* **18** 015303

[29] Wang Y, Wang C, Li K, Li L and Tian Y 2021 *Opt. Quant. Electron.* **53**

[30] Lee H, Chung S, Lee K and Kim D 2008 *New J. Phys.* **10** 093024

[31] Kim D, Lee H, Chung S and Lee K 2009 *New J. Phys.* **11** 063050

[32] Galkin A L, Korobkin V V, Romanovsky M Yu and Shiryaev O B 2008 *Phys. Plasmas* **15** 023104

[33] Galkin A L, Korobkin V V, Romanovsky M Y and Shiryaev O B 2011 *ICONO* 2010*: International Conference on Coherent and Nonlinear Optics*, (SPIE) vol. 7993, pp. 337–47

[34] Corde S, Ta Phuoc K, Lambert G, Fitour R, Malka V, Rousse A, Beck A and Lefebvre E 2013 *Rev. Mod. Phys.* **85** 1

[35] Lee K, Cha Y H, Shin M S, Kim B H and Kim D 2003 *Phys. Rev. E* **67** 026502